ACS Macro Letters

pubs.acs.org/macroletters Letter

Triboelectric Nanogenerators: Enhancing Performance by Increasing the Charge-Generating Layer Compressibility

Junho Jang,[#] Chungryong Choi,[#] Keon-Woo Kim, Yoichi Okayama, Ju Hyun Lee, Javier Read de Alaniz, Christopher M. Bates,* and Jin Kon Kim*

Cite This: *ACS Macro Lett.* 2022, 11, 1291−1297 Read Online

ACCESS | Metrics & More | Article Recommendations | Supporting Information

ABSTRACT: Triboelectric nanogenerators (TENGs) have received significant attention for next-generation wearable electronics due to their simple device structure and low cost. Although the performance of TENGs is intimately tied to compressibility effects in the charge-generating layer, achieving high compressibility with conventional elastomers is challenging because molecular entanglements place a lower bound on the softness of cross-linked networks. Here, we demonstrate that bottlebrush elastomers are efficient charge-generating layers that improve the output performance of TENGs, including voltage, current, and surface potential, by minimizing entanglements and decreasing the compressive modulus (E). For example, a cross-linked bottlebrush with poly(dimethylsiloxane) side chains yielded TENGs with an output voltage (120 V) more than two times larger than a linear PDMS network (55 V). In conclusion, this study highlights the advantage of designing new charge-generating layers with improved compressibility to enhance TENG performance.

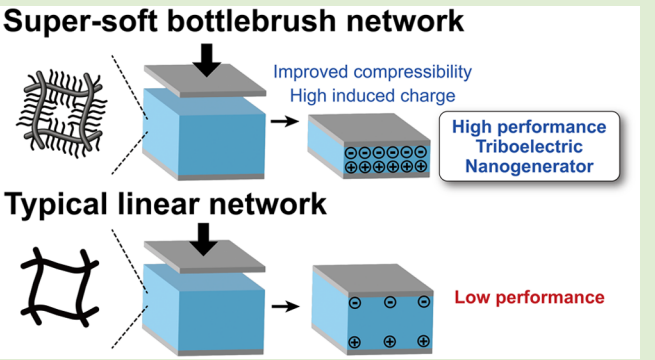

Motivated by applications such as the Internet of Things (IoT), the field of nanoenergy has made significant progress over the past 20 years. A key advance was the development of nanogenerators that convert small-scale (e.g., nano) mechanical movement into electrical energy.[1] Triboelectric nanogenerators (TENGs) are one example that turn motion from energy sources such as wind,[2,3] water,[4−8] and body movement[9] into an electrical signal based on triboelectrification and electrostatic induction. Because this type of electrical energy extracted from dynamic mechanical movement can be used directly as a power supply or stored for later use, TENGs have been applied in a variety of fields, including human−machine interfacing,[10] healthcare monitoring,[11−13] and self-powered sensors.[14−17] In particular, TENGs provide a number of advantages in wearable electronics[18−21] due to their simple device structure and portable energy packaging.[22,23]

To improve the output performance of TENGs, significant research has focused on surface engineering by controlling contact area[24−27] and the compressibility of the charge-generating layer via microstructuring.[28] A larger contact area creates more charge, whereas higher compressibility (i.e., smaller compressive modulus E) increases the amount of charge induced at the surface−collector interface. Although some research groups have investigated the impact of both effects in tandem on the output performance of TENGs,[23−27] they were not controlled independently. In order to systematically improve the performance of TENGs, it is necessary to analyze each factor independently. Poly(dimethylsiloxane) (PDMS) is an ideal material platform to isolate the effects of compressibility because it is a common elastomer with an easily controlled modulus by changing cross-linking density. However, since commercially available PDMS forms linear network structures after curing, the modulus (or compressibility) is limited by molecular entanglements to roughly >1 MPa. Moreover, the cross-link density cannot be lowered *ad infinitum* because a low gel fraction would result in viscous flow or relaxation that is unsuitable for use in TENG devices.

To address this challenge, here we demonstrate that polymer architecture can be used to maximize compressibility without sacrificing a high gel fraction. Our study leverages bottlebrush elastomers, which suppress chain entanglements, an effect that significantly lowers the modulus compared to conventional linear polymer networks.[29−35] Using a simple light-based synthesis method, cross-linked bottlebrush elastomers with PDMS side chains were produced spanning different stiffnesses (E = 0.42−2.60 MPa) by adjusting the ratio of bottlebrush PDMS macromonomer to cross-linker. In addition to providing a tunable platform for controlling mechanical

Received: September 10, 2022
Accepted: October 19, 2022

Downloaded via UNIV OF CALIFORNIA SANTA BARBARA on November 1, 2022 at 15:36:06 (UTC).
See https://pubs.acs.org/sharingguidelines for options on how to legitimately share published articles.

ACS Publications © XXXX American Chemical Society

https://doi.org/10.1021/acsmacrolett.2c00535
ACS Macro Lett. 2022, 11, 1291−1297

properties, these materials have a sufficiently high gel fraction (>80%) for creating mechanically stable TENGs. TENG output performance increases as E decreases, with cross-linked bottlebrush PDMS exhibiting twice the output voltage (120 V) and charge density (125 μC m^{-2}) compared to an analogous TENG device fabricated with linear PDMS (55 V and 58 μC m^{-2}). These results demonstrate the power of controlling polymer architecture in the context of advanced electronic applications.

Since PDMS accumulates negative charge when contacted,[36] it is widely exploited as a charge-generating layer in TENGs. The most common form of PDMS used in these devices is Sylgard 184, which, after thermal curing, generates a linear polymer network. We hypothesized that a charge-generating (i.e., dielectric) layer with an even lower modulus than can be achieved with Sylgard 184 would create more induced charge because of the increased deformability and narrower gap between the two electrodes at a given applied force, as shown in Figure 1.

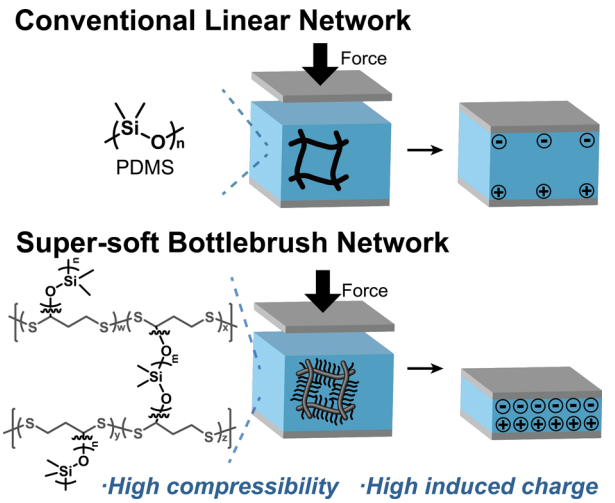

Figure 1. TENG devices based on bottlebrush elastomers should generate more charge at a given applied force due to increased deformability (a lower compressive modulus).

Figure 2a,b plots compressive stress (F) versus compressive strain (s) for BB_1 and BB_5 at different loadings of cross-linker. Note that we denote synthesized bottlebrush samples as BB_X-Y, where X is the number-average molar mass (M_n) of the PDMS macromonomer (i.e., side-chain length in kg/mol) and Y is the mole fraction of cross-linker (also see Materials and Methods section). Compressive moduli ($E = F/s$) were calculated at small F (up to 0.098 MPa, see Figure S1). The value of E for cross-linked bottlebrushes grows from 0.42 to 1.70 MPa as the mole fraction of cross-linker increases from 0.13 to 0.48 with two different side-chain lengths. Longer side chains result in a smaller E as expected based on prior literature.[32−34] Figure 2c shows that E increases with cross-linking density, which is consistent with the phantom network model.[37] From our previous report,[29] with this chemistry, more than 99% of cross-linker forms productive cross-links at the loadings used in BB_1 and BB_5 (15−30 mol %). Notably, high gel fractions (>85%) were achieved with these formulations, resulting in mechanically stable samples that are suitable for the charge generating layer in TENG.

A contact−separation TENG device was fabricated to evaluate the triboelectrification properties of bottlebrush elastomers (Figure 3a). When the indium tin oxide (ITO) electrode contacts the bottlebrush PDMS film, a difference in work function causes static charges with opposite signs on the two surfaces. When the layers begin to compress other, electrons flow from the upper ITO electrode to the lower electrode through an external circuit, generating an electric output signal with a positive sign. After the two layers sufficiently compress, the number of charges equilibrates and charge transfer through the external circuit is complete. As the upper layer starts to separate again, electrons flow from the lower electrode to the upper electrode, generating an electric output signal with a negative sign. Finally, when the device is fully separated, the charge is balanced and a single self-powered cycle is finished. By repeating the contact−separation sequence, mechanical movement is converted into a pulsed AC output (Figure 3b,c).[38] Figure 3d shows the output voltage of BB_1 and BB_5 samples versus the mole fraction of cross-linker. Here, open-circuit voltage (V_{OC}) represents the peak-to-peak voltage as described in Figure S2. Notably, the output voltage of both BB_1 and BB_5 samples increased as the mole fraction of cross-linker decreased due to changes in compressibility (as discussed below). However, when the gel fraction falls below a critical value, output voltage drops dramatically because unreacted PDMS chains leach from the cross-linked PDMS network and contaminate the surface of the opposite electrode during repeated contact (see Figure S3).

The improved performance of TENGs with decreasing E can be explained as follows.[24,39,40]

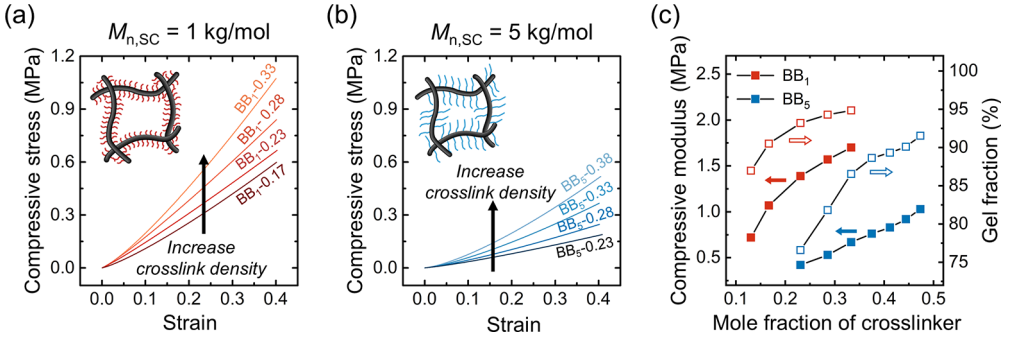

Figure 2. Compressive stress (F) vs strain (s) for PDMS bottlebrush elastomers with side-chain lengths of (a) 1 kg/mol (BB_1) and (b) 5 kg/mol (BB_5) at various cross-link densities. A lower cross-linking density and higher $M_{n,SC}$ decreases E. (c) Plots of E (closed symbols) and gel fraction (open symbols) versus mole fraction of the cross-linker for BB_1 and BB_5 samples.

https://doi.org/10.1021/acsmacrolett.2c00535
ACS Macro Lett. 2022, 11, 1291−1297

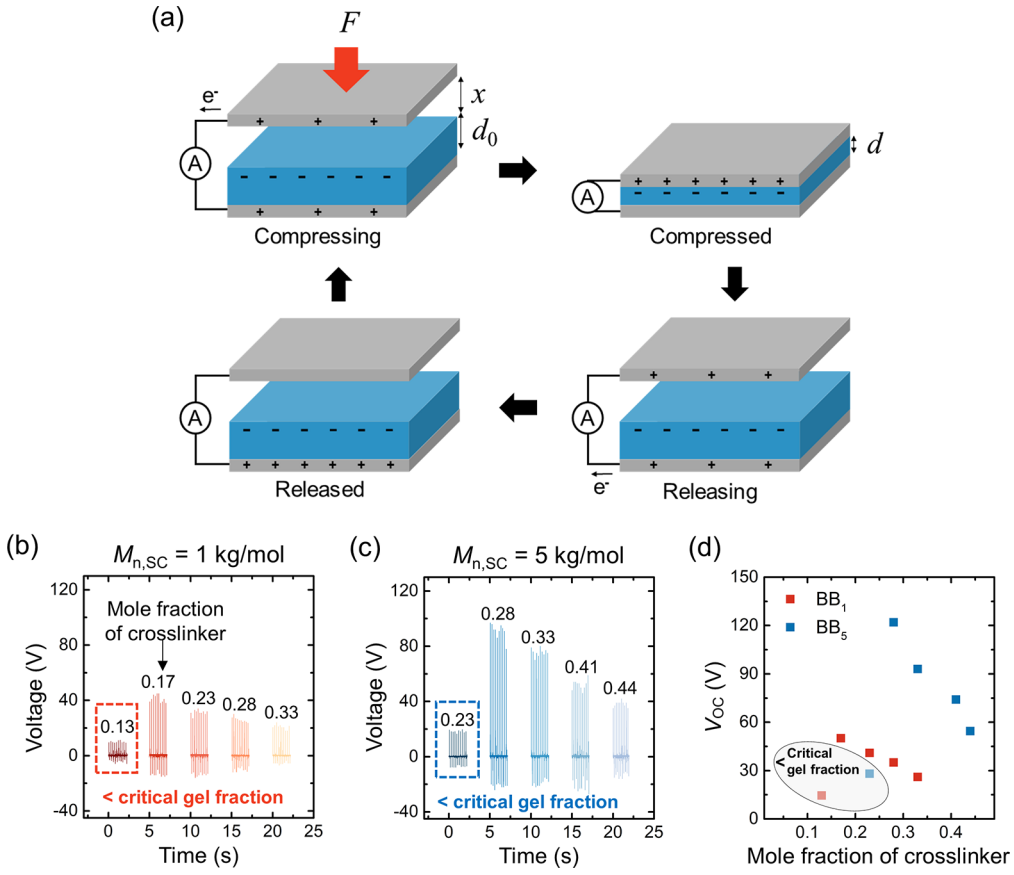

Figure 3. (a) Illustration of the TENG mechanism in contact−separation mode. F: applied stress, x: air gap, d_0: initial thickness, d: compressed thickness. (b, c) Voltage vs time for cross-linked bottlebrush PDMS with side-chain lengths of (b) 1 kg/mol (BB_1) and (c) 5 kg/mol (BB_5). (d) Plot of open-circuit voltage (V_{OC}, peak-to-peak) vs mole fraction of the cross-linker for BB_1 and BB_5 samples. Output voltage increases with decreasing E when the gel fraction is above a critical value (90% for BB_1 and 80% for BB_5). Samples below the critical gel point are marked with an opaque ellipse.

$$V_{OC} = \frac{Q}{C} = \frac{\sigma x}{\varepsilon_0} \tag{1}$$

$$\sigma = \frac{\varepsilon_0 \varepsilon_r \Delta V}{d} \tag{2}$$

In eqs 1 and 2, V_{OC}, Q, and C represent the open circuit output voltage, triboelectric charge, and capacitance, respectively, σ is the charge density, x is the air gap between the electrode and dielectric layer, ε_0 and ε_r are the vacuum permittivity and relative permittivity of the charge-generating layer, and d and ΔV are the compressed thickness and surface potential difference of the charge generating layer, respectively. From eqs 1 and 2, V_{OC} is

$$V_{OC} = \frac{\varepsilon_r \Delta V x}{d} \tag{3}$$

where d is directly related to the compressive modulus (E) at small F according to Young's equation[41]

$$d = d_0\left(1 - \frac{F}{E}\right) \tag{4}$$

with d_0 representing the initial thickness of the dielectric layer, F is the applied compressive stress (0.098 MPa), and E is the compressive modulus. From eqs 3 and 4,

$$\frac{1}{V_{oc}} = \frac{d_0}{\varepsilon_r \Delta V x}\left(1 - \frac{F}{E}\right) = \frac{A}{\Delta V} - \frac{B}{\Delta V E} \tag{5}$$

and

$$\frac{\Delta V}{V_{oc}} = A - \frac{B}{E} \tag{6}$$

where $A = \frac{d_0}{\varepsilon_r x}$ and $B = \frac{d_0 F}{\varepsilon_r x}$. Here, we fixed the values of x, d_0, and F for all experiments. Further, ε_r is similar for every sample because they all share the same chemical structure PDMS.

From eq 6, $\Delta V/V_{OC}$ is a function of E. ΔV is the induced charge formed on the surface when ITO contacts a PDMS charge generating layer. The measured ΔV for BB_1, BB_5, and LN depends on the mole fraction of cross-linker (Figure S4), where conventional (linear) cross-linked PDMS is denoted LN-Y with Y the weight fraction of curing agent. As shown in Figure 4, a linear relationship between $\Delta V/V_{OC}$ and $1/E$ was obtained for all samples. The output voltage in TENGs clearly increases with decreasing E as long as the gel fraction of the charge generating layer is higher than the critical value for each sample. The different slopes (red, blue, and black fit lines) in Figure 4 are within error but could arise from slightly variable compositions (i.e., backbone chemistry), although they are all predominantly PDMS. The calculated values of B/A (~0.1 MPa) in Figure 4 are almost the same, regardless of sample type (Table S1), which is consistent with the prediction of eq

https://doi.org/10.1021/acsmacrolett.2c00535
ACS Macro Lett. 2022, 11, 1291−1297

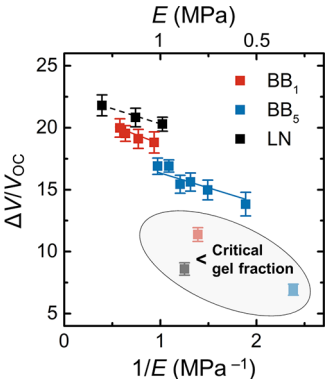

Figure 4. Plot of $\Delta V/V_{OC}$ vs $1/E$ for BB_1, BB_5, and LN. Samples below the critical gel point are marked with a gray ellipse.

6, because B/A should be equal to the applied stress (F = 0.098 MPa).

Figure 5a–c more clearly shows the effect of chain architecture on TENG output performance. LN-0.05 and BB_5-0.28 were chosen as representative examples for each architecture (linear and bottlebrush, respectively) as these formulations exhibited the best performance (see Figure S5 and Table S2 in the Supporting Information). The output performance (voltage, current, and charge density) of cross-linked bottlebrush PDMS is more than two times better than linear PDMS. Figure 5d summarizes the changes in voltage and average peak power with external load resistance. The voltage increases with resistance according to Ohm's law, and the power is maximized when impedance is matched between the TENG and load. Consequently, cross-linked bottlebrush PDMS exhibits a maximum output power of 0.72 mW at a resistance of 20 MΩ. When connected to a TENG and rectifier without capacitors, the power generated from the bottlebrush PDMS network lit 60 green LEDs compared with only 15 with a linear cross-linked PDMS network (Figure 5e).

To a first approximation, the bottlebrush architecture improves the performance of TENGs precisely because it lowers the modulus. However, another consequence of changing architecture appears to be a different surface potential (ΔV, Figure S4). Together, these effects cause a modest difference in the behavior of linear and bottlebrush systems, that is, they do not fall on a common fit line in Figure 4. Even if the trends were identical, the ability of bottlebrush elastomers to soften linear networks by a factor of 10–100 could be quite advantageous in the context of TENGs; swelling with solvent would introduce problems such as leaching and a change in performance over time.

In summary, triboelectric nanogenerators fabricated from bottlebrush elastomers provide more than twice the output performance compared to conventional cross-linked PDMS. This improvement is due to a lower compressive modulus that arises from molecular architecture effects. These results highlight the power of leveraging polymer architecture to control material properties that are important in next-generation devices and advanced technology.

MATERIALS AND METHODS

Materials: Cross-linked bottlebrush PDMS samples were synthesized by a light-mediated method in the absence of the additives to minimize the effect of impurities on TENG performance.[29] Two PDMS macromonomers were synthesized with different molar masses ($M_{n,SC}$ = 1 and 5 kg/mol) as well as a PDMS cross-linker ($M_{n,CL}$ = 5 kg/mol). Conventional (linear) PDMS was prepared from Sylgard 184 (Dow Corning). Indium tin oxide-coated poly(ethylene terephthalate) (PET; ITO-PET) with 60 Ω/sq and ITO-coated glass (ITO-glass) with 15 Ω/sq were purchased from Sigma-Aldrich and Asahi Glass Co, respectively.

Sample preparation: To measure the compressive modulus (E) of cross-linked bottlebrush PDMS samples, a given macromonomer and cross-linker were mixed at various ratios (10–50 mol % of cross-linker

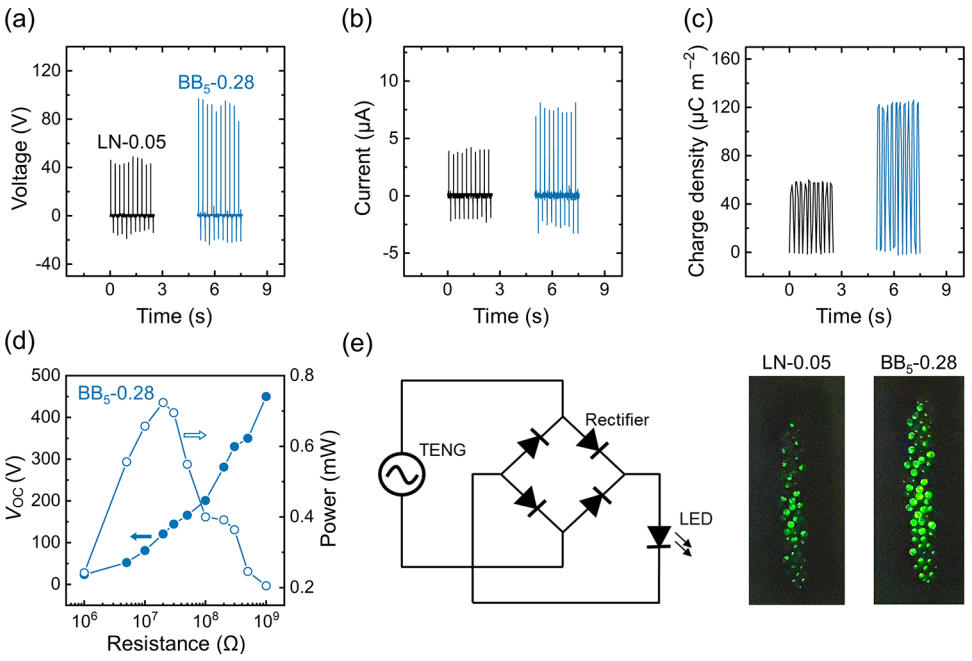

Figure 5. Comparison of TENG output performance with linear (LN-0.05) and bottlebrush (BB_5-0.28) PDMS networks: (a) voltage, (b) current, and (c) charge density vs time. (d) Plots of the voltage and power versus load resistance for BB_5-0.28. (e) Electric circuit for lightening green LEDs (left). The bottlebrush sample lit four times more LEDs than linear PDMS (right).

https://doi.org/10.1021/acsmacrolett.2c00535
ACS Macro Lett. 2022, 11, 1291–1297

relative to PDMS macromonomer). After the mixture was degassed, it was poured into a mold and cured under UV light. Similarly, linear cross-linked PDMS samples were prepared by mixing and curing with various ratios of the Sylgard 184 base to curing agent (3 to 20 wt % of curing agent to base). We denote synthesized bottlebrush samples as BB_X-Y, where X is the number-average molar mass (M_n) of the PDMS macromonomer (i.e., side chain length in kg/mol) and Y is the mole fraction of cross-linker (see Figure S6). Conventional cross-linked linear PDMS is denoted as LN-Y, where Y is the weight fraction of the curing agent in commercially available Sylgard 184.

To prepare TENG devices based on cross-linked bottlebrush PDMS, mixtures of PDMS macromonomer and cross-linker were drop cast on 1 × 1 cm^2 ITO glass slides and exposed to 365 nm light at an intensity of 500 mW/cm^2 (Model L9588, Hamamatsu Co.) under ambient air. For TENG devices based on conventional cross-linked PDMS, Sylgard 184 was prepared with air bubbles completely removed in a vacuum chamber. Mixtures were spin coated on 1 × 1 cm^2 ITO glass slides and thermally cured at 80 °C for 2 h. The thickness of all samples was 600 μm, as confirmed by scanning electron microscopy operating at 3 kV (FE-SEM, Hitachi S-4800; see Figure S7). To measure E, cross-linked bottlebrush and conventional PDMS samples with a diameter of 5 mm and a thickness of 600 μm were punched out. TENG devices with a size of 1 × 1 cm^2 were fabricated by inserting the charge-generating layer (bottlebrush or conventional PDMS) between lower (ITO-glass) and upper (ITO-PET) electrodes. Gel fractions were calculated as $w_{hex}/w_0 \times 100$, where w_{hex} is the weight of a sample after soaking in n-hexane for 24 h and w_0 is the weight before swelling.

TENG output performance: Voltage and current were measured with an oscilloscope (Tektronix, TBS2102). Charge density was measured using a high-resistance electrometer (Keithley, Model 6517). For the periodic application of pressure by touch, a homemade contact machine (SPG Co., Ltd. Model No. S8KA6B) was used to apply mechanical force (1 kgf) at 4 Hz frequency. In order to eliminate the position dependence of the device, 100 kΩ was connected in parallel to the oscilloscope (10 MΩ), and the other side was connected in series with 10 MΩ and 0−3 GΩ to measure general and power measurements, respectively. Since a 10 MΩ probe connected in parallel did not affect the overall circuit resistance, the voltage of the low resistor was measured by an oscilloscope with a 10 MΩ probe.

■ ASSOCIATED CONTENT

Supporting Information

The Supporting Information is available free of charge at https://pubs.acs.org/doi/10.1021/acsmacrolett.2c00535.

Compressive moduli and potential differences of PDMS bottlebrush networks, TENG devices based on a PDMS layer with a low gel fraction, reactive scheme and chemical structure of PDMS bottlebrush networks, SEM image of the charge generating layer (PDF)

■ AUTHOR INFORMATION

Corresponding Authors

Jin Kon Kim − *National Creative Research Initiative Center for Hybrid Nano Materials by High-level Architectural Design of Block Copolymer, Department of Chemical Engineering, Pohang University of Science and Technology (POSTECH), Pohang 37673, Republic of Korea;* orcid.org/0000-0002-3872-2004; Email: jkkim@postech.ac.kr

Christopher M. Bates − *Department of Chemistry and Biochemistry, Materials Department, Materials Research Laboratory, and Department of Chemical Engineering, University of California, Santa Barbara, California 93106, United States;* orcid.org/0000-0002-1598-794X; Email: cbates@ucsb.edu

Authors

Junho Jang − *National Creative Research Initiative Center for Hybrid Nano Materials by High-level Architectural Design of Block Copolymer, Department of Chemical Engineering, Pohang University of Science and Technology (POSTECH), Pohang 37673, Republic of Korea*

Chungryong Choi − *Department of Chemistry and Biochemistry and Materials Department, University of California, Santa Barbara, California 93106, United States; Department of Polymer Science and Engineering, Kumoh National Institute of Technology, Gumi, Gyeongbuk 39177, Republic of Korea*

Keon-Woo Kim − *National Creative Research Initiative Center for Hybrid Nano Materials by High-level Architectural Design of Block Copolymer, Department of Chemical Engineering, Pohang University of Science and Technology (POSTECH), Pohang 37673, Republic of Korea*

Yoichi Okayama − *Materials Research Laboratory, University of California, Santa Barbara, California 93106, United States*

Ju Hyun Lee − *National Creative Research Initiative Center for Hybrid Nano Materials by High-level Architectural Design of Block Copolymer, Department of Chemical Engineering, Pohang University of Science and Technology (POSTECH), Pohang 37673, Republic of Korea*

Javier Read de Alaniz − *Department of Chemistry and Biochemistry, University of California, Santa Barbara, California 93106, United States;* orcid.org/0000-0003-2770-9477

Complete contact information is available at: https://pubs.acs.org/10.1021/acsmacrolett.2c00535

Author Contributions

#These authors contributed equally to this work. CRediT: **Junho Jang** conceptualization (equal), data curation (equal), formal analysis (equal); **Chungryong Choi** conceptualization (equal), data curation (equal), formal analysis (equal); **Keon-Woo Kim** conceptualization (equal), data curation (equal), formal analysis (equal); **Yoichi Okayama** conceptualization (equal), data curation (equal), methodology (equal), validation (equal); **Ju Hyun Lee** conceptualization (equal), data curation (equal), formal analysis (equal); **Javier Read de Alaniz** funding acquisition (equal), investigation (equal), project administration (equal); **Christopher M. Bates** conceptualization (equal), funding acquisition (equal), project administration (equal), supervision (equal), writing-review & editing (equal); **Jin Kon Kim** funding acquisition (equal), project administration (equal), writing-review & editing (equal).

Notes

The authors declare no competing financial interest.

■ ACKNOWLEDGMENTS

J.K.K. acknowledges financial support from the National Creative Research Initiative Program supported by the National Research Foundation (No. 2022R1A3A3002149). The research reported here was supported by the National Science Foundation under Award No. CMMI-2053760 (C.M.B.) and partially supported by the BioPACIFIC Materials Innovation Platform of the National Science Foundation under Award No. DMR-1933487.

REFERENCES

(1) Fan, F.-R.; Tian, Z.-Q.; Lin Wang, Z. Flexible Triboelectric Generator. *Nano Energy* **2012**, *1* (2), 328−334.
(2) Wang, S.; Mu, X.; Wang, X.; Gu, A. Y.; Wang, Z. L.; Yang, Y. Elasto-Aerodynamics-Driven Triboelectric Nanogenerator for Scavenging Air-Flow Energy. *ACS Nano* **2015**, *9* (10), 9554−9563.
(3) Chen, B.; Yang, Y.; Wang, Z. L. Scavenging Wind Energy by Triboelectric Nanogenerators. *Adv. Energy Mater.* **2018**, *8* (10), 1702649.
(4) Nie, J.; Wang, Z.; Ren, Z.; Li, S.; Chen, X.; Lin Wang, Z. Power Generation from the Interaction of a Liquid Droplet and a Liquid Membrane. *Nat. Commun.* **2019**, *10* (1), 2264.
(5) Xu, M.; Zhao, T.; Wang, C.; Zhang, S. L.; Li, Z.; Pan, X.; Wang, Z. L. High Power Density Tower-Like Triboelectric Nanogenerator for Harvesting Arbitrary Directional Water Wave Energy. *ACS Nano* **2019**, *13* (2), 1932−1939.
(6) Yang, X.; Xu, L.; Lin, P.; Zhong, W.; Bai, Y.; Luo, J.; Chen, J.; Wang, Z. L. Macroscopic Self-Assembly Network of Encapsulated High-Performance Triboelectric Nanogenerators for Water Wave Energy Harvesting. *Nano Energy* **2019**, *60*, 404−412.
(7) Xu, W.; Zheng, H.; Liu, Y.; Zhou, X.; Zhang, C.; Song, Y.; Deng, X.; Leung, M.; Yang, Z.; Xu, R. X.; Wang, Z. L.; Zeng, X. C.; Wang, Z. A Droplet-Based Electricity Generator with High Instantaneous Power Density. *Nature* **2020**, *578* (7795), 392−396.
(8) Xu, L.; Pang, Y.; Zhang, C.; Jiang, T.; Chen, X.; Luo, J.; Tang, W.; Cao, X.; Wang, Z. L. Integrated Triboelectric Nanogenerator Array Based on Air-Driven Membrane Structures for Water Wave Energy Harvesting. *Nano Energy* **2017**, *31*, 351−358.
(9) Yi, F.; Lin, L.; Niu, S.; Yang, P. K.; Wang, Z.; Chen, J.; Zhou, Y.; Zi, Y.; Wang, J.; Liao, Q.; Zhang, Y.; Wang, Z. L. Stretchable-Rubber-Based Triboelectric Nanogenerator and Its Application as Self-Powered Body Motion Sensors. *Adv. Funct. Mater.* **2015**, *25* (24), 3688−3696.
(10) Chen, J.; Zhu, G.; Yang, J.; Jing, Q.; Bai, P.; Yang, W.; Qi, X.; Su, Y.; Wang, Z. L. Personalized Keystroke Dynamics for Self-Powered Human-Machine Interfacing. *ACS Nano* **2015**, *9* (1), 105−116.
(11) Ouyang, H.; Tian, J.; Sun, G.; Zou, Y.; Liu, Z.; Li, H.; Zhao, L.; Shi, B.; Fan, Y.; Fan, Y.; Wang, Z. L.; Li, Z. Self-Powered Pulse Sensor for Antidiastole of Cardiovascular Disease. *Adv. Mater.* **2017**, *29* (40), 1703456.
(12) Lin, Z.; Chen, J.; Li, X.; Zhou, Z.; Meng, K.; Wei, W.; Yang, J.; Wang, Z. L. Triboelectric Nanogenerator Enabled Body Sensor Network for Self-Powered Human Heart-Rate Monitoring. *ACS Nano* **2017**, *11* (9), 8830−8837.
(13) Lin, Z.; Yang, J.; Li, X.; Wu, Y.; Wei, W.; Liu, J.; Chen, J.; Yang, J. Large-Scale and Washable Smart Textiles Based on Triboelectric Nanogenerator Arrays for Self-Powered Sleeping Monitoring. *Adv. Funct. Mater.* **2018**, *28* (1), 1704112.
(14) Wu, H.; Huang, Y.; Xu, F.; Duan, Y.; Yin, Z. Energy Harvesters for Wearable and Stretchable Electronics: From Flexibility to Stretchability. *Adv. Mater.* **2016**, *28* (45), 9881−9919.
(15) Fan, F. R.; Tang, W.; Wang, Z. L. Flexible Nanogenerators for Energy Harvesting and Self-Powered Electronics. *Adv. Mater.* **2016**, *28* (22), 4283−4305.
(16) Choi, W.; Yun, I.; Jeung, J.; Park, Y. S.; Cho, S.; Kim, D. W.; Kang, I. S.; Chung, Y.; Jeong, U. Stretchable Triboelectric Multimodal Tactile Interface Simultaneously Recognizing Various Dynamic Body Motions. *Nano Energy* **2019**, *56*, 347−356.
(17) Jang, J.; Kim, D. W.; Lee, J. H.; Choi, C.; Go, M.; Kim, J. K.; Jeong, U. Triboelectric Uv Patterning for Wearable One-Terminal Tactile Sensor Array to Perceive Dynamic Contact Motions. *Nano Energy* **2022**, *98*, 107320.
(18) Ha, M.; Park, J.; Lee, Y.; Ko, H. Triboelectric Generators and Sensors for Self-Powered Wearable Electronics. *ACS Nano* **2015**, *9* (4), 3421−3427.
(19) Chen, X.; Li, X.; Shao, J.; An, N.; Tian, H.; Wang, C.; Han, T.; Wang, L.; Lu, B. High-Performance Piezoelectric Nanogenerators with Imprinted P(Vdf-Trfe)/$BaTiO_3$ Nanocomposite Micropillars for Self-Powered Flexible Sensors. *Small* **2017**, *13* (23), 1604245.
(20) He, X.; Zi, Y.; Guo, H.; Zheng, H.; Xi, Y.; Wu, C.; Wang, J.; Zhang, W.; Lu, C.; Wang, Z. L. A Highly Stretchable Fiber-Based Triboelectric Nanogenerator for Self-Powered Wearable Electronics. *Adv. Funct. Mater.* **2017**, *27* (4), 1604378.
(21) Deng, J.; Kuang, X.; Liu, R.; Ding, W.; Wang, A. C.; Lai, Y.-C.; Dong, K.; Wen, Z.; Wang, Y.; Wang, L.; Qi, H. J.; Zhang, T.; Wang, Z. L. Vitrimer Elastomer-Based Jigsaw Puzzle-Like Healable Triboelectric Nanogenerator for Self-Powered Wearable Electronics. *Adv. Mater.* **2018**, *30* (14), 1705918.
(22) Tang, Q.; Yeh, M.-H.; Liu, G.; Li, S.; Chen, J.; Bai, Y.; Feng, L.; Lai, M.; Ho, K.-C.; Guo, H.; Hu, C. Whirligig-Inspired Triboelectric Nanogenerator with Ultrahigh Specific Output as Reliable Portable Instant Power Supply for Personal Health Monitoring Devices. *Nano Energy* **2018**, *47*, 74−80.
(23) Jiang, D.; Ouyang, H.; Shi, B.; Zou, Y.; Tan, P.; Qu, X.; Chao, S.; Xi, Y.; Zhao, C.; Fan, Y.; Li, Z. A Wearable Noncontact Free-Rotating Hybrid Nanogenerator for Self-Powered Electronics. *InfoMat* **2020**, *2* (6), 1191−1200.
(24) Lee, J. H.; Yu, I.; Hyun, S.; Kim, J. K.; Jeong, U. Remarkable Increase in Triboelectrification by Enhancing the Conformable Contact and Adhesion Energy with a Film-Covered Pillar Structure. *Nano Energy* **2017**, *34*, 233−241.
(25) Fan, F.-R.; Lin, L.; Zhu, G.; Wu, W.; Zhang, R.; Wang, Z. L. Transparent Triboelectric Nanogenerators and Self-Powered Pressure Sensors Based on Micropatterned Plastic Films. *Nano Lett.* **2012**, *12* (6), 3109−3114.
(26) Wang, S.; Lin, L.; Wang, Z. L. Nanoscale Triboelectric-Effect-Enabled Energy Conversion for Sustainably Powering Portable Electronics. *Nano Lett.* **2012**, *12* (12), 6339−6346.
(27) Chun, J.; Kim, J. W.; Jung, W.-s.; Kang, C.-Y.; Kim, S.-W.; Wang, Z. L.; Baik, J. M. Mesoporous Pores Impregnated with Au Nanoparticles as Effective Dielectrics for Enhancing Triboelectric Nanogenerator Performance in Harsh Environments. *Energy Environ. Sci.* **2015**, *8* (10), 3006−3012.
(28) Lee, K. Y.; Chun, J.; Lee, J.-H.; Kim, K. N.; Kang, N.-R.; Kim, J.-Y.; Kim, M. H.; Shin, K.-S.; Gupta, M. K.; Baik, J. M.; Kim, S.-W. Hydrophobic Sponge Structure-Based Triboelectric Nanogenerator. *Adv. Mater.* **2014**, *26* (29), 5037−5042.
(29) Choi, C.; Self, J. L.; Okayama, Y.; Levi, A. E.; Gerst, M.; Speros, J. C.; Hawker, C. J.; Read de Alaniz, J.; Bates, C. M. Light-Mediated Synthesis and Reprocessing of Dynamic Bottlebrush Elastomers under Ambient Conditions. *J. Am. Chem. Soc.* **2021**, *143* (26), 9866−9871.
(30) Choi, C.; Okayama, Y.; Morris, P. T.; Robinson, L. L.; Gerst, M.; Speros, J. C.; Hawker, C. J.; Read de Alaniz, J.; Bates, C. M. Digital Light Processing of Dynamic Bottlebrush Materials. *Adv. Funct. Mater.* **2022**, *32* (25), 2200883.
(31) Cai, L.-H.; Kodger, T. E.; Guerra, R. E.; Pegoraro, A. F.; Rubinstein, M.; Weitz, D. A. Soft Poly(Dimethylsiloxane) Elastomers from Architecture-Driven Entanglement Free Design. *Adv. Mater.* **2015**, *27* (35), 5132−5140.
(32) Daniel, W. F. M.; Burdyńska, J.; Vatankhah-Varnoosfaderani, M.; Matyjaszewski, K.; Paturej, J.; Rubinstein, M.; Dobrynin, A. V.; Sheiko, S. S. Solvent-Free, Supersoft and Superelastic Bottlebrush Melts and Networks. *Nat. Mater.* **2016**, *15* (2), 183−189.
(33) Mukherjee, S.; Xie, R.; Reynolds, V. G.; Uchiyama, T.; Levi, A. E.; Valois, E.; Wang, H.; Chabinyc, M. L.; Bates, C. M. Universal Approach to Photo-Crosslink Bottlebrush Polymers. *Macromolecules* **2020**, *53* (3), 1090−1097.
(34) Self, J. L.; Sample, C. S.; Levi, A. E.; Li, K.; Xie, R.; De Alaniz, J. R.; Bates, C. M. Dynamic Bottlebrush Polymer Networks: Self-Healing in Super-Soft Materials. *J. Am. Chem. Soc.* **2020**, *142* (16), 7567−7573.
(35) Vatankhah-Varnoosfaderani, M.; Daniel, W. F. M.; Zhushma, A. P.; Li, Q.; Morgan, B. J.; Matyjaszewski, K.; Armstrong, D. P.; Spontak, R. J.; Dobrynin, A. V.; Sheiko, S. S. Bottlebrush Elastomers: A New Platform for Freestanding Electroactuation. *Adv. Mater.* **2017**, *29* (2), 1604209.

https://doi.org/10.1021/acsmacrolett.2c00535
ACS Macro Lett. 2022, 11, 1291−1297

(36) Li, J.; Shepelin, N. A.; Sherrell, P. C.; Ellis, A. V. Poly(Dimethylsiloxane) for Triboelectricity: From Mechanisms to Practical Strategies. *Chem. Mater.* **2021**, *33* (12), 4304−4327.
(37) Rubinstein, M.; Colby, R. H.*Polymer Physics*; Oxford University Press: New York, 2003; Vol. *23*.
(38) Kang, X.; Pan, C.; Chen, Y.; Pu, X. Boosting Performances of Triboelectric Nanogenerators by Optimizing Dielectric Properties and Thickness of Electrification Layer. *RSC Adv.* **2020**, *10* (30), 17752−17759.
(39) Niu, S.; Wang, Z. L. Theoretical Systems of Triboelectric Nanogenerators. *Nano Energy* **2015**, *14*, 161−192.
(40) Lee, J.-H.; Hinchet, R.; Kim, T. Y.; Ryu, H.; Seung, W.; Yoon, H.-J.; Kim, S.-W. Control of Skin Potential by Triboelectrification with Ferroelectric Polymers. *Adv. Mater.* **2015**, *27* (37), 5553−5558.
(41) Hearn, E. J., Chapter 1 - Simple Stress and Strain. In *Mechanics of Materials 1*, 3rd ed.; Hearn, E. J., Ed. Butterworth-Heinemann: Oxford, 1997; pp 1−26.

Recommended by ACS

Honeycomb-Patterned Polyimide-Based Triboelectric Nanogenerator with Excellent Thermal Stability and Enhanced Electrification Performance

Van-Tien Bui, Huynh Nhat Do, *et al.*
JULY 27, 2022
ACS APPLIED ENERGY MATERIALS
READ

Laminated Triboelectric Nanogenerator for Enhanced Self-Powered Pressure-Sensing Performance by Charge Regulation

Renjie Xu, Zhen Wen, *et al.*
AUGUST 24, 2022
ACS APPLIED MATERIALS & INTERFACES
READ

Separation-Free Planar Interconnection for Thermo-electrochemical cells

Ju Hyeon Kim, Tae June Kang, *et al.*
SEPTEMBER 28, 2022
ACS APPLIED ENERGY MATERIALS
READ

Active Deformable and Flexible Triboelectric Nanogenerator Based on Super-Light Clay

Kaixuan Wang, Zhong Lin Wang, *et al.*
AUGUST 30, 2022
ACS APPLIED ELECTRONIC MATERIALS
READ

Get More Suggestions >

https://doi.org/10.1021/acsmacrolett.2c00535
ACS Macro Lett. 2022, 11, 1291−1297